Nature Environment and Pollution Technology
An International Quarterly Scientific Journal

p-ISSN: 0972-6268
(Print copies up to 2016)
e-ISSN: 2395-3454

Vol. 24 | No. 3 | Article ID B4277 | 2025

Original Research Paper

https://doi.org/10.46488/NEPT.2025.v24i03.B4277

Open Access Journal

Single-Step Green Method of Synthesis of Activated Carbon from Lignocellulosic Biomass Waste of *Jacaranda mimosifolia* for Sustainable Water Purification

Vishal Haribhai Patel[1,2], Abdul Gani[1]† and Anamika Paul[3]

[1]School of Engineering, Galgotias University, Plot No.2, Sector 17-A, Yamuna Expressway, Greater Noida-201310, Uttar Pradesh, India

[2]Amity University, Room No. G05, J3 Block, Amity University, Noida-201313, Uttar Pradesh, India

[3]WSP Global Inc., 1st Floor, FC24, Sector 16A, Noida-201306, Uttar Pradesh, India

†Corresponding author: Abdul Gani; abdul.gani@galgotiasuniversity.edu.in

Abbreviation: Nat. Env. & Poll. Technol.
Website: www.neptjournal.com

Received: 17-10-2024
Revised: 13-12-2024
Accepted: 22-12-2024

Key Words:

Activated carbon
Lignocellulosic biomass waste
Green synthesis
Water purification
Jacaranda mimosifolia

Citation for the Paper:

Patel, V. H., Gani, A. and Paul, A., 2025. Single-step green method of synthesis for activated carbon from lignocellulosic biomass waste of *Jacaranda mimosifolia* for sustainable water purification. *Nature Environment and Pollution Technology*, 24(3), B4277. https://doi.org/10.46488/NEPT.2025.v24i03.B4277

Note: Since 2025, the journal has adopted the use of Article IDs in citations instead of traditional consecutive page numbers. Each article is now given individual page ranges starting from page 1.

ABSTRACT

Abundant lignocellulosic biomass components have been a source of inspiration for designing complex materials with high surface area and potent applications in a wide variety of commercial products, including water purification, biosensors, catalysis, and others. Billion tons of lignocellulosic biomass waste are produced in a year. This lignocellulosic biomass waste could be a good source of precursor for activated carbon and other carbon-based nanomaterials. Activated carbon was prepared from Seed pods of lignocellulosic biomass of *Jacaranda mimosifolia,* which was treated as waste using a single-step green method of synthesis. Synthesized activated carbon was characterized using high-resolution scanning electron microscopy (HRSEM), X-ray diffraction (XRD), Fourier transform infrared spectroscopy (FTIR), N_2 adsorption/desorption, and Zeta potential. It was evident that the synthesis method was free from chemical use and thus eco-friendly. We have reported maximum removal of heavy metal, lead ion (Pb^{+2}), and dye Eriochrome Black T (EBT) using prepared activated carbon was 58.77 and 286.56 $mg \cdot g^{-1,}$ respectively. The adsorption was rapid, with 97% of Pb^{+2} and 90% of EBT adsorption accomplished within 60 min. The synthesized material could be used in the design of a filter for sustainable water purification.

INTRODUCTION

Many organic and inorganic water-soluble pollutants are discharged into water bodies, giving rise to serious environmental problems. The wastewater produced from various industries such as manufacturing, printing, textile (Yao et al. 2020), chemicals, electronics, and pharmaceutical industries (Özdemir et al. 2019) carries a noticeable quantity of pollutants, including dyes and heavy metals. This has remained a major environmental challenge. They are responsible for the seepage of different pollutants, such as dyes (Tonato et al. 2019), heavy metals, and phenols (Mohammed et al. 2018), into the aquatic environment without proper removal. Both heavy metals and dyes are envisaged to be some of the most dangerous pollutants in water systems as they exhibit mutagenic, immunogenic, carcinogenic, and teratogenic characteristics (Azari et al. 2019) and also cause serious environmental and health problems for aquatic flora, fauna, and finally human health (Yin et al. 2019).

Dyes are used in varied sectors, including textile, paper, leather, dyestuff, printing, plastic, cosmetics, and coatings, because of their low cost, brightness, and high resistance against environmental conditions (Reck et al. 2018). Moreover, dyes were very stable to light, temperature, microbial attack, and even at low concentrations optically active and detectable (Bello et al. 2018),

causing a very acute impact on water bodies (dos Santos et al. 2018).

Industries generating a massive quantity of heavy metals-laden wastewater contain arsenic, cadmium, lead, cobalt, copper, chromium, mercury, zinc, iron, manganese, nickel, and others. These effluents are released into water bodies without proper treatment (Liu et al. 2019, Dobrowolski et al. 2019), and poisonous at low concentrations (Ali et al. 2019), could be bio-accumulated/magnified along with food chains, and pose hazards to human health (Que et al. 2019) and found within the different environmental compartments (Alonso-Magdalena et al. 2019). Owing to the mentioned impacts on different biota, a strong demand for water purification from heavy metals and dyes becomes crucial.

The key techniques that are used to remove pollutants from the water phase include physical and chemical processes including coagulation/flocculation (Hou et al. 2019), precipitation (Chen et al. 2018), ultrafiltration (Kavitha et al. 2019), photo-oxidation (Du & Chen 2018), electrodialysis (Nemati et al. 2017), electrocoagulation (Doggaz et al. 2019), membrane separation (Hosseini et al. 2018), ion exchange (Feng et al. 2019), forward osmosis (Qiu & He 2019), electrochemical oxidation of Wastewater (Rai & Sinha 2022), irradiation (Ghobashy & Elhady 2017), and adsorption (Wei et al. 2021). The biological processes include phytoextraction (Napoli et al. 2019) and biological degradation (Jacob et al. 2018).

In the past few years, bio templates from natural sources like extracts of various plant components have been a source of inspiration for designing complex materials with high surface area, which have potent applications in a wide variety of commercial products, including filters for water purification, biosensors, catalysis, and others.

Biosorption, using bio-wastes for the elimination of different water pollutants, is an eco-friendly, economical, and efficient technique (Gupta et al. 2018) that limits the concentration of different water pollutants to the acceptable limits recommended by different federal regulations (Krstić et al. 2018). Numerous benefits are attained due to the recycling of these biomasses, including waste minimization, and could rectify different ecological as well as environmental problems (Gupta et al. 2019). Adsorption using a low-cost and sustainable biosorbent derived from biomass provides an alternative to a circular economy (Madeła & Skuza 2021).

Jacaranda mimosifolia used in the study belongs to the botanical family Bignoniaceae reported to be native of South America. The jacaranda has been cultivated in almost every part of the world and used in numerous metropolises in tropical and sub-tropical countries as an ornamental tree (Mostafa et al. 2014) (Ragsac et al. 2019). *Jacaranda mimosifolia* can be categorized as a medium-sized tree which is usually less than 10 m tall and can reach 12-15 m under ideal conditions (*Agroforestree database*). Seed pods, drying dark brown, have a compressed-elliptical shape and are 3.5–8.5 cm long. Seeds are surrounded by a thin membrane, usually 0.8–1.4 cm long. Its seed pods were not edible and attractive to birds as they lacked a pleasing color or scent. Therefore, upon ripening, they dry and fall, generating a large amount of organic biomass over the soil. Very limited studies were found in the literature related to the use of *Jacaranda mimosifolia* seed pods (JMSP) for the removal of pollutants from water or wastewater.

In the present study, activated carbons (biosorbent) for water treatment have been synthesized using biomass of JMSP to investigate the adsorption performance of Pb^{+2} and Eriochrome Black T (EBT) in aqueous solution. The effect of various operational parameters, kinetics, thermodynamics, adsorption isotherms and adsorption mechanism were investigated by combining different methods, including high-resolution scanning electron microscopy (HRSEM), X-ray diffraction (XRD), Fourier transforms infrared spectroscopy (FTIR), N_2 adsorption/desorption and Zeta potential.

MATERIALS AND METHODS

Chemicals and Reagents Used

The JMSP was collected from local city gardens of greater Noida, India. Reagents used in experiments were analytical grade, and no further processing was carried out before use. Unless specified, the deionized water (18.2 MΩ·cm) was used during all experiments. The standard stock solutions of 1000 $mg.L^{-1}$ were prepared for metal ion Pb^{+2} and EBT. Table 1 describes the specification and chemical structure of EBT used for the study. The pH of the solution was adjusted using 0.01-1 M HCl and NaOH.

Preparation of Activated Carbon

The seeds were removed from the collected JMSP before processing them. First, collected JMSP were washed with tap water to remove the residual dirt, sand, and other soluble impurities, then washed with deionized water 4 times. Washed JMSP were dried in a laboratory oven at 70°C for 24 h until constant weight. The dried JMSP was ground using an electronic blender and sieved into the particles < 177 µm and stored in plastic bottles. The sieved JMSP powder was placed into the specially designed reactor under the inert atmosphere with an N_2 flow rate of 0.001 $m^3 \cdot min^{-1}$ with a heating rate maintained at 300°C·min^{-1} to the final temperature of 1950°C, which was maintained for 05 min (carbonization) followed by activation at 1950°C

Table 1: Specification and Chemical Structure of Eriochrome Black T (EBT).

Dye Name	IUPAC Name	Chemical Formula & MoLecular Weight	Chemical Structure	λ_{max} (nm)
Eriochrome Black T (EBT)	sodium;4-[(1-hydroxy naphthalene-2-yl) hydrazinylidene]-7-nitro-3-oxonaphthalene-1-sulfonate CAS Number 1787-61-7	$C_{20}H_{12}N_3O_7SNa$ 461.381 g·moL^{-1}	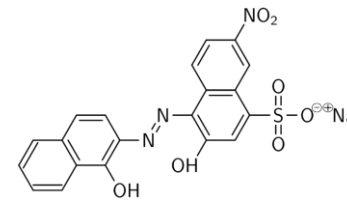	526

Table 2: Proximate analysis of synthesized JMSP activated carbon.

Particular	Moisture % on a dry basis	Volatile matter % on a dry basis	Ash % on a dry basis	Fixed carbon % on a dry basis
JMSP AC	6.67	22.26	3.03	74.71

under CO_2 with flow rate of 0.001 $m^3 \cdot min^{-1}$ for 05 min. The temperature of 1950^oC was maintained for a total time of 10 min, 05 min for carbonization, and 05 min for activation. The prepared activated carbon was left to cool to room temperature and washed with deionized water; the activated carbon was separated using a 0.45 µm nylon membrane filter. The activated carbon obtained was dried at 110^oC for 24 h, cooled to room temperature in a desiccator, and kept in airtight bottles for further analysis. The prepared activated carbon was labeled as JMSP AC. The single-step synthesis method for the production of activated carbon (biosorbent) was efficient and free from the use of chemical, thus eco-friendly. Additionally, the synthesis process operated with flexibility and scalability. The quantitative analysis (Table 2) confirms the higher conversion of available elemental carbon from lignocellulosic biomass to activated carbon using the proposed synthesis method.

The percent yield of JMSP AC was determined from the relation:

$$Yield(\%) = \frac{w_{ac}}{w_0} \times 100 \quad \ldots(1)$$

where w_{ac} and w_0 were the final JMSP AC dry weight (g) and the precursor dry weight (g), respectively.

Adsorption Studies

The efficacy of the synthesized JMSP AC was tested as an adsorbent for the Pb^{+2} and EBT sorption from aqueous solutions in the batch experiments. All experiments were triplicate, and the mean of these were reported with the control experiment in the same operating conditions without adding adsorbent. Different standard solutions (10ppm, 25 ppm, 50 ppm, 75 ppm, 100 ppm, 125 ppm, 150 ppm) of Pb^{+2} metal ion and (10 ppm, 25 ppm, 50 ppm, 100 ppm, 200 ppm, 300 ppm, 400 ppm, 500 ppm) for EBT dye were prepared and kept in the refrigerator to maintain the constant volume and concentration. The adsorption experiments were carried out in a 250 ml flask containing 100 ml of metal and dye solution of various concentrations, dosage of JMSP AC, and contact time at natural solution pH. Samples were shaken in a thermostat incubator at 200 rpm for 2 h. The residual metal ion concentration was determined using ICP-OES (Agilent Technologies 700 series), and that of the dye was determined using a UV-VIS spectrophotometer (Agilent Carry 100 UV-Vis). The amount of metal ion and dye adsorbed per unit mass of adsorbent was calculated according to the equation:

$$Q_e = \frac{(C_0 - C_e)V}{W} \quad \ldots(2)$$

Where Q_e was the amount of metal ion/dye adsorbed on biosorbent (mg·g^{-1}), and C_0 and C_e were the initial and equilibrium concentrations of metal ion/dye solution (mg·L^{-1}). V - volume of metal ion/dye solution (L), and W - amount of JMSP AC biosorbent (g).

The following equation determined the % removal:

$$\text{Removal } (\%) = \frac{(C_0 - C_e)}{C_0} \times 100 \quad \ldots(3)$$

The adsorption kinetics were done at 25 ^0C and natural pH with concentrations at 100 and 250 mg·L^{-1} for metal ion and dye, respectively. The samples were analyzed at predefined time intervals, and metal ion/dye uptake on biosorbent at time t was determined using Eq. 4

$$Q_t = \frac{(C_0 - C_t)V}{W} \quad \ldots(4)$$

Where C_t (mg·L^{-1}) - concentration of metal ion/dye at any time.

The adsorption isotherm data were analyzed using four different types of adsorption isotherm models, including the Langmuir, Freundlich, Temkin, and Redlich-Peterson (R-P); the kinetic models used were pseudo-first-order, pseudo-second-order, and intraparticle diffusion (Table 3).

Furthermore, to elucidate the adsorption thermodynamics, $Pb^{+2,}$ and EBT adsorption was conducted at different

Table 3: Adsorption isotherms and kinetic models.

Models	Equation	Parameters
Langmuir	$Q_e = \frac{Q_m K_L C_e}{1+K_L C_e}$	K_L = constant related to the affinity of binding sites (L·mg^{-1})
Freundlich	$Q_e = K_F C_e^{\frac{1}{n}}$	K_F = constant related to adsorption capacity (L·g^{-1}), n = constant related to the intensity of adsorption
Temkin	$Q_e = \frac{RT}{B_T}\ln(A_T C_e)$	A_T = equilibrium binding constant (L·g^{-1}), R = universal gas constant (8.314 J·moL^{-1} K^{-1}), R = universal gas constant (8.314 J·moL^{-1} K^{-1}), T = absolute temperature (K), B_T = constant related to adsorption heat (J·moL^{-1})
Redlich-Peterson (R-P)	$Q_e = \frac{K_R C_e}{1+a_R C_e^{\,g}}$	K_R = R-P constant (L·g^{-1}) a_R = R-P constants (L·mg^{-1}) g = exponent related to surface heterogeneity
Pseudo-first order	$Q_t = Q_e\,(1 - e^{-k_1 t})$	k_1 = equilibrium rate constant (min^{-1})
Pseudo-second order	$Q_t = \frac{{Q_e}^2 k_2 t}{1+Q_e k_2 t}$	k_2 = equilibrium rate constant (g·mg^{-1}·min^{-1})
Intraparticle Diffusion model	$Q_t = k_i t^{1/2} + C$	k_i = rate constant mg·g^{-1}·min$^{-0.5}$, C = boundary layer thickness

temperatures in the range of 25 to 40°C with 0.8 g·L^{-1} of adsorbent suspended in 50 mL 50 ppm Pb^{+2}/EBT solution agitated at 200 rpm for 2 h. The various thermodynamic parameters at equilibrium, including Gibb's free energy change (ΔG^0), enthalpy change (ΔH^0), and entropy change (ΔS^0), were calculated based on the adsorbate concentration C_e (mg·L^{-1}) and adsorption capacity Q_e (mg·g^{-1}) in solution in equilibrium at different temperatures.

Biosorbent Regeneration

Regeneration of the used JMSP biosorbent was carried with 0.2 M HNO_3 to desorb the sequestered Pb^{+2} and EBT, using a solid/liquid ratio of 3 g·L^{-1} for 2 h. Subsequently, the biosorbent was separated using a 0.45 µm nylon filter. The filtrate was analyzed for desorbed Pb^{+2} and EBT, while the separated biosorbent was washed with milli-Q water 3 times and then used for resorption study after drying in the oven at 110°C for 12 h.

Characterization of JMSP AC Biosorbent

To elucidate the underlying adsorption mechanisms and active binding sites, JMSP biosorbent were characterized using a variety of physicochemical and spectroscopic approaches before and after Pb^{+2}/ EBT adsorption (i.e., pristine JMSP biosorbent and Pb^{+2}/EBT loaded JMSP AC). The surface electric property of JMSP biosorbent was examined by a Malvern Zetasizer (Nano Series) and pH drift method (Faria et al. 2004). Textural characterization of the JMSP AC was carried out by N_2 adsorption at 77 K using Quantachrome Autosorb IQ Surface area analyzer. The XRD diffractogram of the JMSP was recorded using CuKα radiation (λ = 1.54184 Å) at 30 kV and 10 mA in the range of 2θ from 5° to 90° (Bruker, Germany). The surface morphological and elemental properties of JMSP were investigated by a high-resolution scanning electron microscopy (Thermo scientific Apreo S) coupled with an EDX. Furthermore, the functional groups on the JMSP surface were identified by FTIR spectroscopy in the range of 500–4000 cm^{-1} wavenumber (PerkinElmer Frontier).

RESULTS AND DISCUSSION

Yield and Surface Electric Property

The activated carbon synthesized in this study had an approximate yield of 26.80 %, which was in agreement with the previous work related to the processing of JMSP for activated carbon (Treviño-Cordero et al. 2013) (Elizalde-González & Hernández-Montoya 2009). The zeta potential measurement revealed (Table 4) that the surface charge for prepared activated carbon (JMSP AC), activated carbon loaded with Pb^{+2} (JMSP AC-Pb^{+2}) and EBT (JMSP AC-EBT) were -16.2 mV, -12.8 mV and -26.9 mV respectively. The result showed that the stability of the JMSP AC-EBT complex was more stable than the JMSP AC-Pb^{+2} complex compared to JMSP AC. The increase in zeta potential after adsorption with Pb^{+2} ion indicates the binding of metal ions on the surface of the biosorbent, while the attachment of negatively charged functional groups on the JMSP AC surface resulted in a decrease of zeta potential after EBT adsorption. The point of zero charge (pH_{PZC}) for the synthesized activated carbon was 7.42. With increasing pH, the surface becomes more negatively charged, leading to a stronger electrostatic attraction, while a decrease in the pH results in a more positive charge, leading to stronger repulsion forces (Rambabu et al. 2020).

Table 4: The Zeta potential of JMSP AC before and after Pb^{+2} and EBT adsorption.

Material	Zeta Potential ξ [mV]
JMSP AC	-16.2
JMSP AC-Pb^{+2}	-12.8
JMSP AC-EBT	-26.9

Characterization of Activated Carbons

The N_2 adsorption/desorption isotherms of the prepared JMSP AC are shown in Fig.1. According to isotherm, a progressive increase of relative pressure resulted in increased N_2 volume even at very low relative pressure (inset Fig.1). The adsorption isotherm for prepared JMSP biosorbent belong to type IV isotherm according to the IUPAC classification (Sing et al. 1985), which indicates the mesoporous structure.

The predominant hysteresis loop indicates the adsorption with capillary condensation (Donohue & Aranovich 1998, Thommes et al. 2015). The development of mesoporous distribution of JMSP AC and isotherm at low relative pressure (0.010).

The structure was affirmed by the pore size distribution (Fig.1), as shown most of the pores had sizes between 2.9 to 38 nm, which according to IUPAC classification associated with mesoporous materials. (Sing et al. 1985, Thommes et al. 2015).

Different BET study parameters shown in Table 5 revealed that the mesopore volume was 92% of the total pore volume with a surface area of 136 $m^2 \cdot g^{-1}$. The average pore size of the JMSP AC was 3.10 nm. In the literature, similar structure characteristics were reported with activated carbon prepared from plant-based materials (Danish et al. 2018, Lima et al. 2019, Cunha et al. 2020, Kasperiski et al. 2018, Salomón et al. 2021).

The surface morphological aspects of the synthesized biosorbent by SEM are represented in Fig. 2. The prepared JMSP AC biosorbent (Fig. 2b) observed greater surface irregularity compared to the raw Jacaranda mimosifolia seed pods (Fig. 2a) with even distribution of the cavities over the surface. These pores were favorable to adsorption, as they could increase the adsorption capacity of the adsorbate molecules of Pb^{+2} and EBT. After the Pb^{+2} adsorption on the biosorbent, some metal particles precipitate was observed. The elemental mapping exhibits the intense signal for Pb and O, confirming the microprecipitation of Pb^{+2} on the surface of the biosorbent.

The XRD diffraction study reveals the crystalline property of JMSP (Fig. 3a). The broad peak at $2\theta^0$ of 8-29 characterized various amorphous phases such as

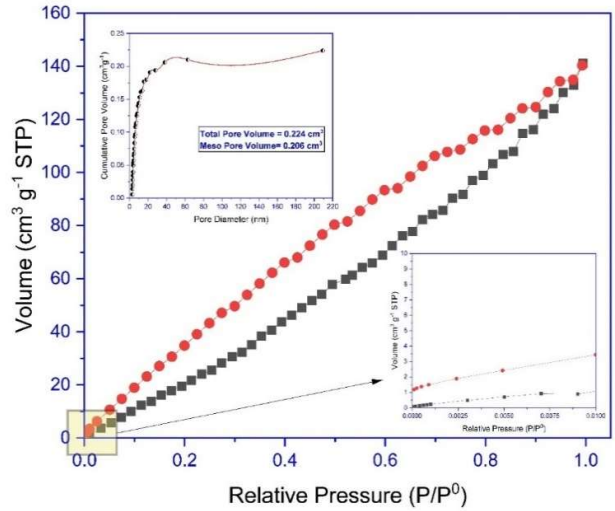

Fig. 1: N_2 adsorption/desorption isotherms of the prepared JMSP AC inset show the pore size.

Table 5: BET study parameters of prepared JMSP AC.

	D_p (nm)	S_{BET} [m^2g^{-1}]	V_T [cm^3g^{-1}]	V_μ [cm^3g^{-1}]	V_m [cm^3g^{-1}]	V_m/V_T [%]	V_μ/V_T [%]
JMSP AC	3.10	136	0.224	0	0.206	92	0

D_p = average pore diameter, S_{BET} = BET surface area, V_T = total pore volume, V_μ = micropore volume, V_m = mesopore volume, V_m/V_T = percentage of mesopore, V_μ/V_T = percentage of micropore

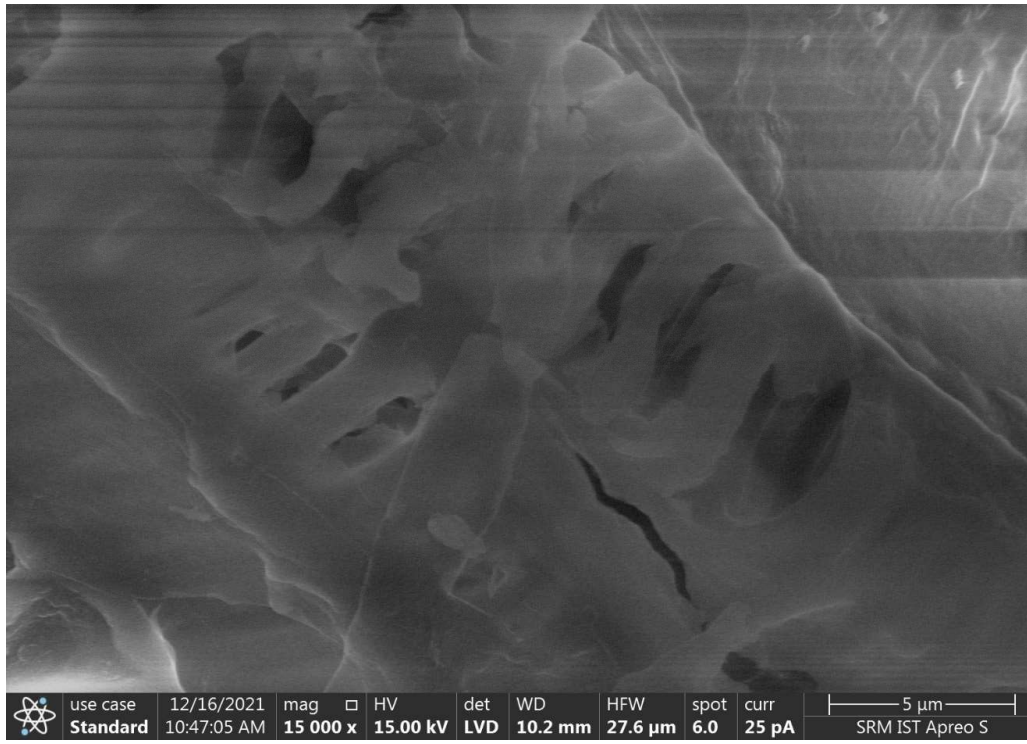

(a)

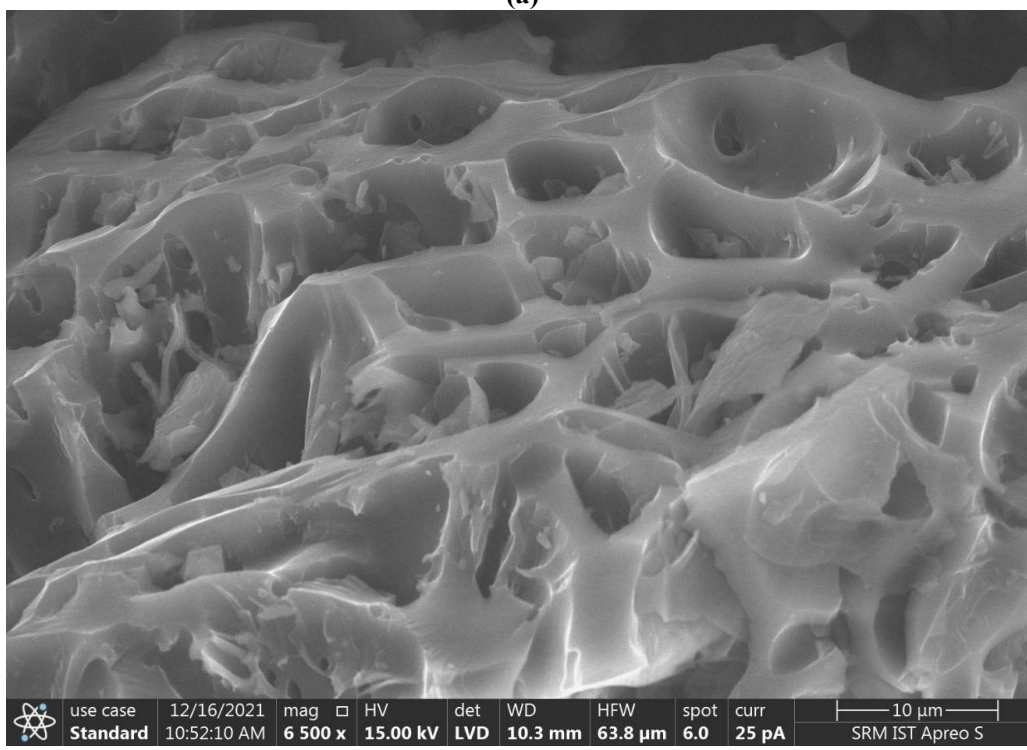

(b)

Fig. 2: SEM images of (a) Raw Jacaranda mimosifolia seed pods (JMSP) (b) prepared JMSP AC biosorbent.

hemicellulose, lignin, and amorphous cellulose of the prepared biosorbent. The distinct reflection at $2\theta^0$ of 16 and 26, along with unresolved doublet at 22 and 23, corresponded to starch of *Jacaranda mimosifolia* seed pod biosorbent (Sandhu & Lim 2008) (Patiño-Rodríguez et al. 2020). Cellulose from the JMSP has a well-defined crystal structure with absorption peaks in XRD diffractogram at 2θ angles of 16° corresponding to crystal plane (101) and 23° (002), respectively. The presence of all the peaks in the diffractogram pattern of the JMSP AC indicated the successful formation of the desired porous carbon. It was elucidated that after the adsorption of Pb^{+2} and EBT on JMSP AC, the diffractogram showed broader and weaker reflections, confirming the reduced crystallinity of JMSP AC. This should be due to the binding of JMSP AC with Pb^{+2} and EBT, resulting in the disorientation of the crystalline regions of JMSP AC because of hydrogen bond breakage to prevent the disorientation of crystalline regions (Moyo et al. 2017). These amorphous regions were responsible for the adsorption of Pb^{+2} and EBT on biosorbent.

The changes in various functional groups on the JMSP AC biosorbent before and after adsorption of Pb^{+2} and EBT were confirmed from FTIR spectra (Fig. 3b). The complex composition of JMSP AC biosorbent could be realized from the various adsorption bands observed. The FTIR spectra of JMSP AC biosorbent exhibited broad weak adsorption bands for stretching vibration of O–H with free hydroxyl at 3660 cm^{-1}, twin sharp bands at 2981 cm^{-1} and 2973 cm^{-1} at 2924 cm^{-1} for C–H in alkanes, C=O stretch in saturated carbonyl at 1715 cm^{-1}, bending vibrations of N–H in primary amines at 1591 cm^{-1}, stretching of acyl C–O at 1286 cm^{-1} and 1206 cm^{-1}, stretching of amines C–N at 1109 cm^{-1}, C–O in primary alcohol at 1028 cm^{-1} and bending of alkene C–H at 839 cm^{-1}. This confirmed the existence of various functional groups in JMSP AC, e.g., hydroxyl, amine, carboxyl and alkene. After the adsorption with Pb^{+2} and EBT on biosorbents, all such bands were removed for Pb^{+2} adsorption and weakened for EBT suggesting the binding of Pb^{+2} and EBT to the functional groups (Hufton et al. 2021) (Ren et al. 2022) which strongly favor the adsorption of pollutants on the biosorbent. Furthermore, following Pb^{+2} and EBT adsorption, the prominent peaks at 2981 cm^{-1} and 2973 cm^{-1} were decreased and displaced, suggesting that hydrogen bonding may be associated with the Pb^{+2} and EBT sorption process by JMSP AC. The peak at 1591 cm^{-1} may have been caused by the JMSP AC stretching vibration, which shifted following the adsorption of Pb^{+2} and EBT, suggesting that π-π type interaction may have been involved in the adsorption process by JMSP AC.

Adsorption performance of JMSP AC for Pb^{+2} and EBT

Effect of pH on adsorption: It was evident that the pH of the solution plays a pivotal role in adsorption studies due to its effect on the electrostatic interaction between adsorbates and adsorbents. In the present study, the effect of pH on the removal of heavy metal Pb^{+2} and dye EBT was determined in the pH range from 2-9. For pH>9, under basic conditions the formation of the precipitation of salts occurred as their hydroxide can influence the adsorption process, therefore adsorption study was conducted for pH up to 9. Lead ions (Pb^{+2}) showed the maximum adsorption of about 59.24 $mg{\cdot}L^{-1}$ at pH 5 (Fig. 4a) and for EBT, pH 6 was found to be optimum with maximum adsorption of 289.32 $mg{\cdot}L^{-1}$ (Fig. 4b).

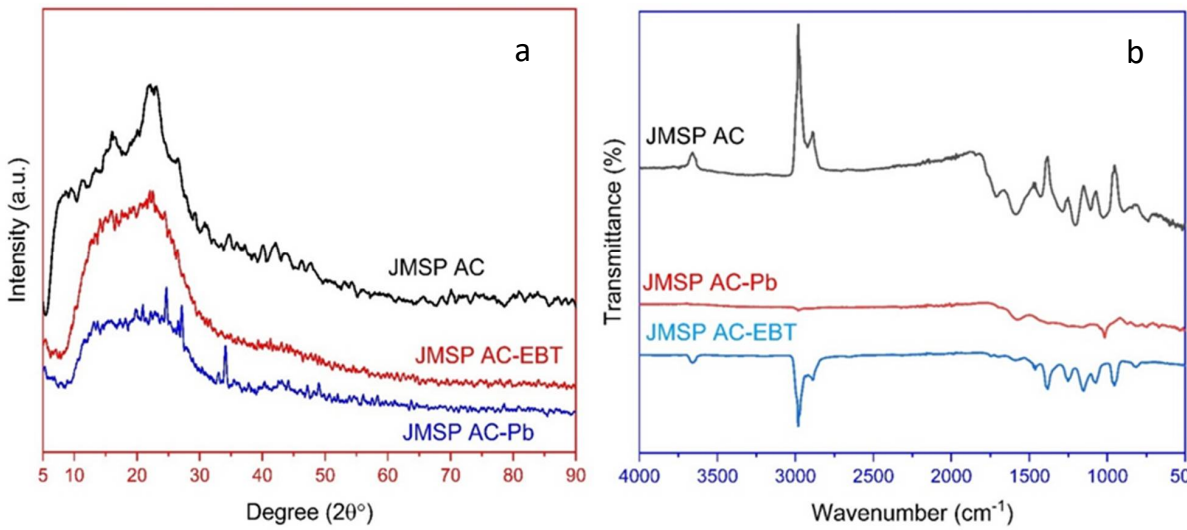

Fig. 3: (a) XRD diffractogram of JMSP AC before and after Pb^{+2} and EBT adsorption. (b) FTIR Spectra of JMSP AC before and after Pb^{+2} and EBT.

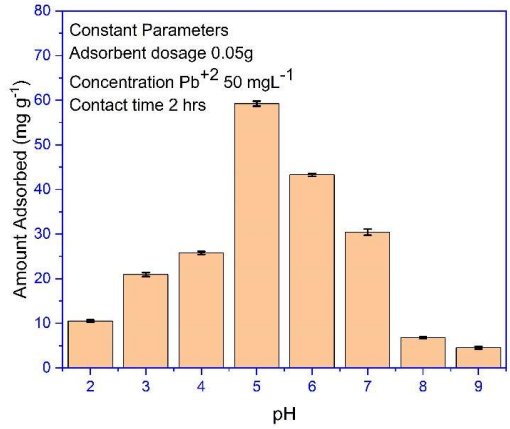

(a)

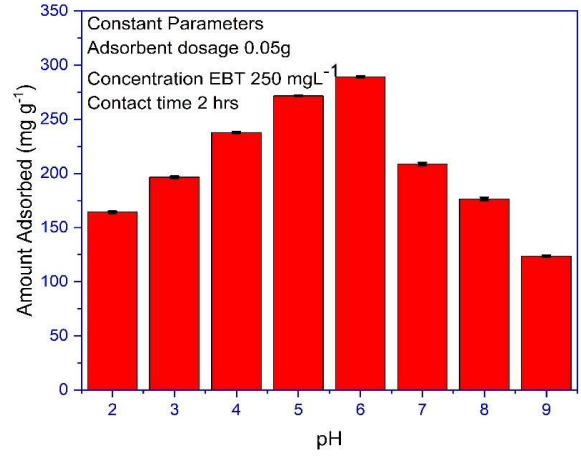

(b)

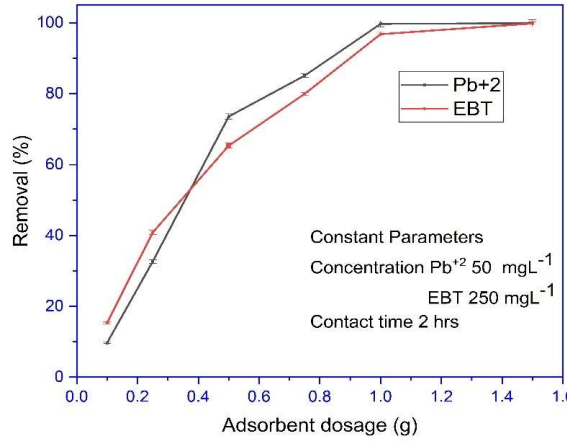

(c)

Fig. 4: Effect of pH (a & b) and dosage (c) for the adsorption of Pb^{+2} and EBT on JMSP AC.

Effect of dosage on adsorption: The minimum possible dosage for the optimum adsorption of Pb^{+2} and EBT was determined, and the amount of biosorbent dosage was varied 0.1 g, 0.25 g, 0.50 g, 0.75 g, 1.0 g, and 1.5 g in 100 ml of 50 mg·L^{-1} Pb^{+2} and 250 mg·L^{-1} EBT solution. The adsorption was increased with the amount of biosorbent dosage for the Pb^{+2} ions and EBT, which was found to be 32.62% and 40.83% at a dosage of 0.25 g and reached 85.10% and 79.96% at a dosage of 0.50 g (Fig. 4c). The adsorption reached to about 100% removal of metal ion Pb^{+2} and dye EBT at 1.5 g of JMSP AC. However, the overall adsorption of Pb^{+2} is lower than the EBT on the biosorbent.

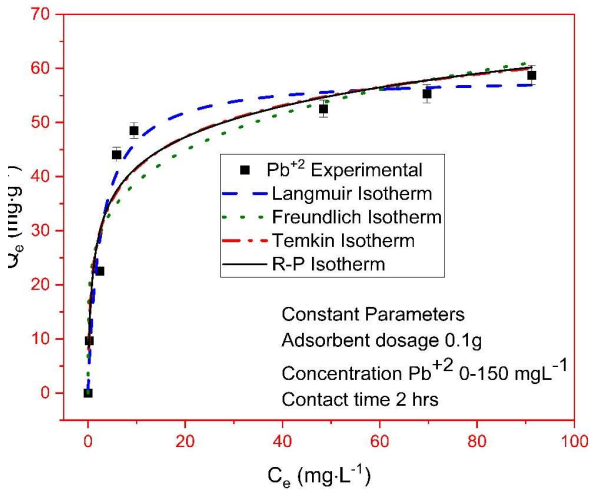

(a)

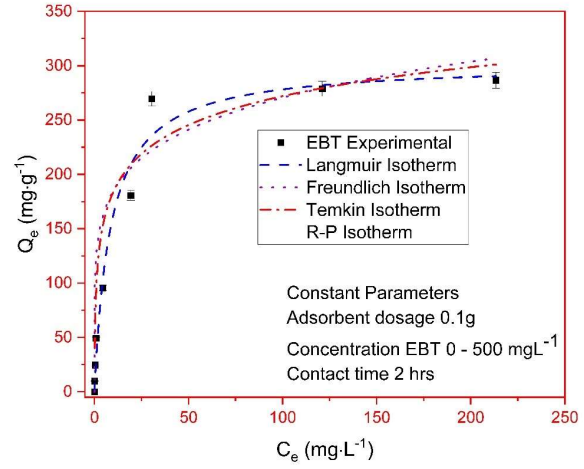

(b)

Fig. 5: Adsorption isotherm of Pb+2 (a) and EBT (b) adsorption on JMSP AC with nonlinear fitting to langmuir, freundlich, temkin and R-P models.

As can be observed trend of adsorption with the adsorbent dosage, with increase in dosage, the adsorption increases and reaches to maximum for 1.5 g. These observations evince that adsorption is directly proportional to the amount of the adsorbent dosage.

Adsorption Isotherms: In the equilibrium study, the nonlinear isotherm models of Langmuir, Freundlich, Temkin, and Redlich-Peterson (R-P) were realized to determine the mode of adsorption and interaction between the metal ion Pb^{+2} and dye EBT. Fig. 5 depicted the nonlinear fitting for the above models for Pb^{+2} (Fig. 5a) and EBT (Fig. 5b), and Table 6 illustrated the values of constants and correlation coefficient for all four isotherm models. The maximum Pb^{+2} adsorption capacity of JMSP AC was determined to be 58.77 mg·$g^{-1,}$ and the R-P adsorption model provided the best description (Fig. 5a, Table 6) with a correlation coefficient (R^2) of 0.9998. For EBT adsorption, the maximum adsorption capacity was 286.56 mg·$g^{-1,}$ and a similar nonlinear R-P adsorption model provided the best description (Fig. 5b, Table 6) with a correlation coefficient (R^2) of 0.9996. The features of both, Langmuir and Freundlich isotherms were incorporated into the R-P model, and it reduces to the Freundlich model if the value of a_{rcin}^{g} was much higher than 1.0 and approaches the Langmuir model when g equals 1.0. This confirmed the multilayer adsorption of Pb^{+2} and EBT on the heterogeneous surface of JMSP AC.

Furthermore, a dimensionless constant, the separation factor (R_L) defined by the following relationship predicting the adsorption nature of the process.

$$R_L = \frac{1}{1+K_L C_0} \quad \ldots(5)$$

where K_L refers to the Langmuir constant and C_0 was the initial concentration of adsorbate in (mg·L^{-1}). The separation factor indicates the nature of adsorption to either be irreversible ($R_L = 0$), unfavorable ($R_L > 1$), linear ($R_L = 1$), or favorable ($0 < R_L < 1$).

In the present study, the experimentally calculated R_L values for the adsorption of Pb^{+2} and EBT on synthesized JMSP AC were 0.0172 - 0.2083 and 0.0164 – 0.4545, respectively. These R_L values confirmed that biosorbent JMSP AC was advantageous for adsorption of Pb^{+2} and EBT from water.

Moreover, values of Freundlich constant n were found to be 4.92 (1/n = 0.203) and 6.01 (1/n = 0.166) for the adsorption of Pb^{+2} and EBT, respectively, suggesting favorable adsorption (0<1/n<1) on the surface of synthesized biosorbent. This encourages the utilization of low-cost JMSP AC for the removal/recovery of heavy metals and dyes from wastewater.

Table 6: Parameters for adsorption isotherm and kinetic models of Pb^{+2} and EBT adsorption by JMSP AC.

Models	Parameter	Pb^{+2}	EBT
Isotherms			
Langmuir	Q_m	58.56	302.1
	K_L	0.38	0.12
	R^2	0.9762	0.9779
Freundlich	K_F	24.41	125.8
	n	4.92	6.01
	R^2	0.9106	0.8617
Temkin	A_T	14.49	12.02
	B_T	8.35	38.36
	R^2	0.9524	0.9859
Redlich-Peterson	K_R	69.65	232.66
	a_R	2.18	1.58
	g	0.86	0.87
	R^2	**0.9998**	**0.9996**
Kinetics			
Pseudo-first order	Q_e	59.51	234.28
	k_1	0.05	0.1
	R^2	**0.9945**	0.9736
Pseudo-second order	Q_e	68.26	253.39
	k_2	9.72×10^{-4}	6.13×10^{-4}
	R^2	0.9813	**0.9967**
Intraparticle Diffusion	k_i	4.17	7.95
	C	17.28	153.57
	R^2	0.7462	0.8799

(Note: Q_e - Equilibrium adsorption capacity, Q_m - Maximum adsorption capacity. Details of other parameters are referred to in Table 3.

Adsorption kinetics: To determine the kinetics of Pb^{+2} and EBT adsorption on JMSP AC, different models, including pseudo-first order, pseudo-second order, and Intraparticle diffusion, were applied. Fig. 6 shows the kinetic fitting for different models and Table 6 represents the various constants for the fitted models along with the correlation coefficient. It was found that the adsorption follows the pseudo-first order and pseudo-second order for the adsorption of Pb^{+2} (Fig 6a, Table 6) and EBT (Fig 6b, Table 6) on the synthesized JMSP AC, respectively, with the correlation coefficient (R^2) 0.9945 and 0.9967. The intercept C for the intraparticle diffusion (Fig 6c, Table 6) for Pb^{+2} and EBT adsorption was 17.28 and 153.57, respectively, evident that the effect of the boundary layer is higher for EBT adsorption than that of Pb^{+2} on the surface of biosorbent. Further, analysis of the kinetic data for the intraparticle diffusion model observed that the plot does not pass through the origin, suggesting that intraparticle diffusion was not the only rate-limiting step for the adsorption of Pb^{+2} and EBT on biosorbent.

The equilibria of the Pb^{+2} and EBT adsorption processes on JMSP AC were readily reached within 180 min, with 97.04% of Pb^{+2} and 90.28% of EBT adsorption reached in the first 60 min (Fig. 6).

The Pb^{+2} and EBT adsorption processes had three phases: in first phase, during first 20 minutes, Pb^{+2} and EBT quickly bound to JMSP AC due to the high availability of the free surface binding sites; during second phase from 20 to 60 minutes, it was gradual decrease in adsorption rate and final third stage start after 60 minutes, which characterize as equilibrium stage with slow uptake of Pb^{+2} and EBT on the biosorbent due to the less free binding sites available as a result of surface saturation of the adsorbent and decreased concentration of Pb^{+2} and EBT in the liquid phase.

Adsorption thermodynamics: The temperature (25 to 40°C) effect on the adsorption of Pb^{+2} and EBT was investigated. Thermodynamic parameters such as free energy change (ΔG^0), enthalpy (ΔH^0), and entropy (ΔS^0) were calculated according to equations.

$$\Delta G^0 = - RT\ln K_d \quad \ldots(6)$$

$$K_d = \frac{Q_e}{C_e} \quad \ldots(7)$$

$$\Delta G^0 = \Delta H^0 - T\Delta S^0 \quad \ldots(8)$$

The parameters ΔH^0 and ΔS^0 were obtained from the slope and intercept of the plot $\ln K_d$ versus 1/T. The thermodynamic parameters are given in Table 7. The ΔG^0 of Pb^{+2} adsorption by JMSP AC biosorbent was -7.39, -5.93, -4.17, and -2.78 $kJ.moL^{-1}$ at 298, 303, 308, and 313 K, respectively. This confirmed that the Pb^{+2} adsorption process became less spontaneous with increased temperature. The ΔH^0 and ΔS^0 were estimated to be -100.22 $kJ.moL^{-1}$ and -0.311 $kJ.K.moL^{-1}$, respectively implied that the Pb^{+2} adsorption by JMSP AC was exothermic and reduced randomness at the solid-liquid interface of the adsorption system.

For EBT adsorption, the ΔG^0 was -9.11, -7.10, -5.39, and -3.67 $kJ.moL^{-1}$ at 298, 303, 308, and 313 K, respectively, indicating the reduced adsorption spontaneity at higher temperatures. The ΔH^0 and ΔS^0 were estimated to be -116.66 $kJ.moL^{-1}$ and -0.361 $kJ.K^{-1}.moL^{-1}$, respectively. The decreased adsorption of Pb^{+2} and EBT by biosorbent at higher temperatures could reduce the thickness of thermal boundary layer for the adsorbed Pb^{+2}/EBT leads to the escape from the JMSP AC surface back into the bulk solution (Rambabu et al. 2020). This probably indicates a poor interplay between adsorbate and various surface functionalities of JMSP AC.

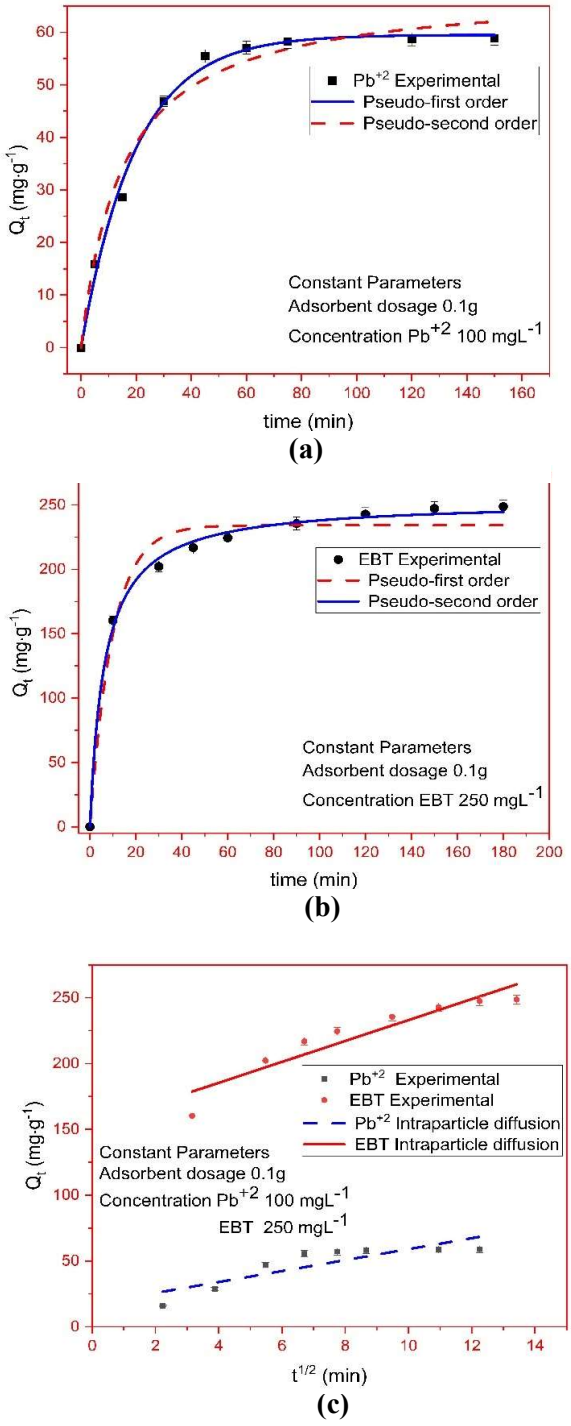

Fig. 6: Adsorption kinetics of Pb+2 (a) and EBT (b) adsorption on JMSP AC with nonlinear fitting to pseudo-first order, pseudo-second order and Intraparticle diffusion (c) kinetic models.

The adsorption mechanism of Pb^{+2} and EBT on JMSP AC biosorbents was explored by examining experimental data through various kinetic models, including pseudo-first order, pseudo-second order, and intraparticle diffusion. The proton quantity could influence the adsorption for Pb^{+2} and EBT, suggesting the surface-active regions on JMSP AC. The various interactions between the surface of JMSP AC and Pb^{+2}/EBT resulted in adsorption, including surface complexation, microprecipitation, and electrostatic attraction (Fig. 7).

Table 7: The thermodynamic parameters of Pb^{+2} and EBT adsorption by JMSP AC biosorbent.

	ΔG^0 [kJ. moL^{-1}]	ΔH^0 [kJ. moL^{-1}]	ΔS^0 [$kJ.K^{-1}$. moL^{-1}]
Pb^{+2} adsorption			
298 K	-7.39	-100.22	-0.311
303 K	-5.93		
308 K	-4.17		
313 K	-2.78		
EBT adsorption			
298 K	-9.11	-116.66	-0.361
303 K	-7.10		
308 K	-5.39		
313 K	-3.67		

Regeneration of biosorbent: Stability and the biosorbent's capacity for regeneration were typically crucial elements in practical applications, which was investigated through six consecutive adsorption-desorption cycles (Fig. 8) using 0.2 M HNO_3 as effective eluting agents for regeneration of the JMSP AC biosorbents. However, plant biomass based biosorbents were inexpensive, widely accessible, and recyclable. It was observed that as the number of regeneration cycles increased, the adsorption efficiency dropped, for Pb^{+2} efficiency was reduced from 83% to 68 % during the first three cycles and further reduced to 39% after the sixth regeneration cycle, whereas for EBT, efficiency was reduced from 92% to 85 % and further reduced to 12% at the end of the sixth regeneration cycle. This suggested that, with the right procedures, the biosorbent may be recycled. To optimize the regeneration process, the eluting agents' solution was stirred at 50-100 rpm for 120 min at 298.15 K, and this helped to minimize pickling of the surface of JMSP AC, which facilitated the reduction of the decline in adsorption efficiency over the cycles.

Comparative studies: Different biosorbents synthesized from lignocellulosic biomass were applied for the removal of heavy metal ion Pb^{+2} and dye EBT from water. Table 8 illustrated the maximum adsorption capacity (Q_m) of different adsorbents for the removal of Pb^{+2} and EBT confirmed that the synthesized biosorbent JMSP AC was much more efficient compared to other adsorbents. The previous study had various limitations in terms of cost-effectiveness, scale-up, energy consumption, regeneration potential, reproducibility, implementation in resource-constrained regions for large-scale water treatment, and

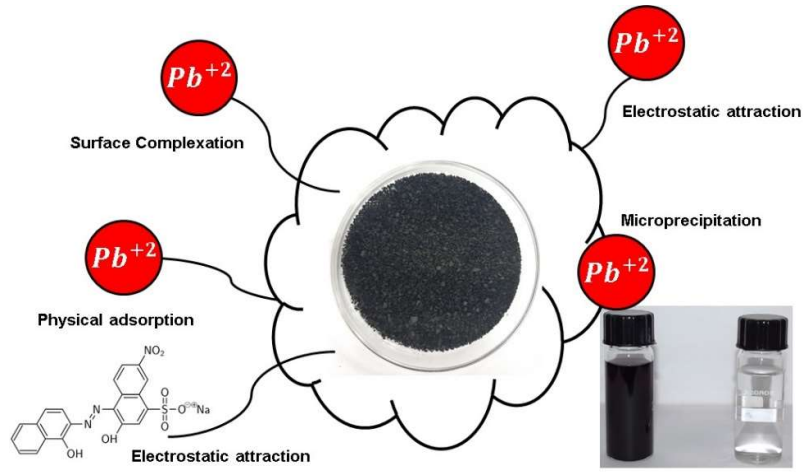

Fig. 7: Schematics of Adsorption mechanism of Pb^{+2} and EBT on JMSP AC.

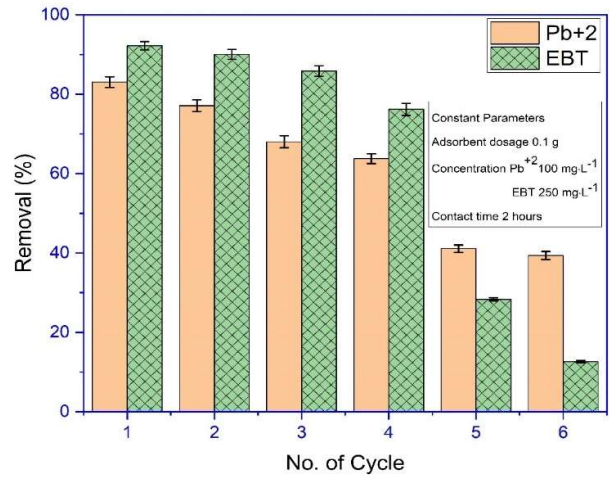

Fig. 8: Sequential adsorption- desorption cycles of the prepared JMSP AC for regeneration.

environmental sustainability. As major synthesis processes used toxic chemicals in their production cycle (Melliti et al. 2023, Eletta et al. 2023, Bumajdad & Hasila 2023, Beyan et al. 2024, Isam et al. 2024, Al-Ma'abreh et al. 2024, Aziz et al. 2019, Abiza et al. 2024, Ali et al. 2022, Ayuba & Sani 2022, El Mansouri et al. 2022, Rath et al. 2024, Sadeghi et al. 2021)) for activated carbon including chemicals used in pre and post-treatment steps. The scalability and reproducibility of disclosed processes has limited scope as insufficient disclosure of entire production process (Mandal et al. 2021, Melliti et al. 2023, Eletta et al. 2023, Bumajdad & Hasila 2023, Isam et al. 2024, Mkilima et al. 2024, Ali et al. 2022, El Mansouri et al. 2022), this prone to the hurdle in adaptation of production processes at commercial scale. Major constraints for implementation of large-scale production of activated carbon include the availability of energy and emission of huge amounts of greenhouse gases (GHG) as major production processes were very energy intensive, these processes had very high specific energy consumption in terms of kilowatt hours (KWH) per kilogram of activated carbon produces which leads to high GHG footprint. In contrast to the above limitations, our single-step green synthesis process addresses major constrain for its adaptability at industrial scale production. First, our process did not require any environmentally hazardous chemicals; secondly, required little energy compared to previously reported processes; and finally, the disclosed production process could easily scale up and reproduce as our study has sufficient disclosure of the entire production process. The cost-effectiveness of our single-step green synthesis process made it easy to adopt for large-scale water treatment facilities for environmental sustainability. Thus, our study

Table 8: The adsorbent JMSP AC comparison of adsorption capacities for Pb+2 and EBT with different adsorbents.

Sr.No.	Pollutants	Adsorbents	Q_m ($mg \cdot g^{-1}$)	Ref.
	Pb^{+2}	Kenaf-based activated carbon (KAC)	11.236	(Mandal et al. 2021)
		activated carbon (date palm fiber)	29.859	(Melliti et al. 2023)
		Activated carbon (*Theobroma tithonia*)	46.95	(Eletta et al. 2023)
		f-activated carbon (palm tree)	4.112	(Bumajdad & Hasila 2023)
		activated carbon (red algae-*Gracilaria changii*)	36.231	(Isam et al. 2024)
		Activated carbon (Teff Straw)	42.97	(Beyan et al. 2024)
		Activated carbon-sodium alginate-oxalate gel particles	53.04	(Li et al. 2024)
		activated carbon (banana peel)	6	(Mkilima et al. 2024)
		Activated Carbon (*Cypress* Fruit)	56.18	(Al-Ma'abreh et al. 2024)
		kenaf-core activated carbon	12.7	(Mandal et al. 2021)
		Chemically activated Jute	25	(Aziz et al. 2019)
		Jacaranda mimosifolia Seed pod Activated Carbon	58.77	present work
	EBT	Activated carbon (*Spartium junceum*)	261.36	(Abiza et al. 2024)
		Chitosan (Shrimp shell)	162.3	(Khnifira et al. 2021)
		Activated carbon (Datura metal seeds)	154.5	(Ali et al. 2022)
		biochar (giant reed)	9.06	(Abdu et al. 2024)
		Activated Carbon (Waste Hemp *Cannabis sativa* L.)	14.025	(El Mansouri et al. 2022)
		graphene (wheat straw)	146.2	(Sadeghi et al. 2021)
		Activated carbon (*Typha* grass)	47.619	(Ayuba & Sani 2022)
		graphene oxide/activated carbon (*Carica papaya* seeds)	51.84	(Rath et al. 2024)
		Nano Carbon (Morus Nigra (Mulberry) Stem)	192.308	(Ahmed et al. 2024)
		Activated Carbon (Pepper Stalks)	55.56	(DOLAŞ 2023)
		Jacaranda mimosifolia Seed pod Activated Carbon	286.56	present work

linked with availability and sustainable management of water (SDG6) and sustainable consumption of natural resources (SDG12) for the production of Activated carbon with a smaller environmental footprint leads to reduced GHG Emissions (SDG13).

Based on the current study, we learned distinct reasons for the high adsorption capacities of the synthesized JMSP AC.

1) The single-step synthesis method produces several types of active sites.
2) Surface hydroxyl groups produce the surface complexation between contaminants.
3) Electrostatic attraction, co-exchanges, microprecipitation, and surface diffusion occur between Pb^{+2} and EBT and prepared biosorbent.
4) The porous architecture of the synthesized biosorbent allowed the adsorption of various contaminants.
5) The adopted single-step synthesis method produces abundant transformation sites responsible for introducing physiochemical partition and stacking of sites to adsorb contaminant molecules.

CONCLUSIONS

In summary, we investigated novel and scalable synthesis of JMSP AC and its application for the removal of contaminants from water and wastewater. The synthesized biosorbent, a waste-to-resource product, manifested efficient adsorption of Pb^{+2} and EBT (Q_m of 58.77 mg-Pb^{+2}/g and 286.56 mg-EBT/g). The adopted single-step synthesis method was more energy efficient and eco-friendly compared to expensive conventional energy-intensive production and treatment processes. The binding sites for Pb^{+2} and EBT were identified as hydroxyl, amine, ether, and carboxyl groups. The underlying adsorption mechanism comprises electrostatic attraction, microprecipitation, diffusion, and complexation. The mechanism provides an understanding of interactions between water pollutants and biosorbents. The study revealed the single-step, eco-friendly, and scalable synthesis method for producing activated carbon (biosorbent) for the removal of heavy metal and dye from water.

ACKNOWLEDGMENTS

We acknowledge the Central research facility at SRM

Institute of Science and Technology, Indian Institute of Technology Delhi, Amity University Uttar Pradesh, and Galgotias University for felicitating the use of scientific Instruments.

REFERENCES

Abdu, M., Babaee, S., Worku, A., Msagati, T.A.M. and Nure, J.F., 2024. The development of Giant reed biochar for adsorption of Basic Blue 41 and Eriochrome Black T. azo dyes from wastewater. *Scientific Reports*, 14 (1), p.18320. DOI.

Abiza, A., Reffas, A., Boubaker, H., Ben Arfi, R., Ghorbel, D., Rafique, M., Bachirou, G.L. and Ghorbal, A., 2024. Comparative analysis of EBT dye removal using *Spartium junceum* and derived activated carbon: experimental and DFT insights. *International Journal of Environmental Analytical Chemistry*, pp.1–27. DOI.

Agroforestry database : a tree reference and selection guide, version 4.0 | CiNii Research, n.d. DOI.

Ahmed, M., Ismaeel, S. and Al-Hyali, E., 2024. Equilibrium and Thermodynamic Studies for the Removal of Eriochrome Black T dye from its Aqueous Solutions using Nano Carbon Prepared from *Morus Nigra* (Mulberry) Stem through two Stages of Carbonization. *Journal of Education and Science*, 33 (2), pp.81–97. DOI.

Ali, H., Khan, E. and Ilahi, I., 2019. Environmental chemistry and ecotoxicology of hazardous heavy metals: Environmental persistence, toxicity, and bioaccumulation. *Journal of Chemistry*, pp.1–14. DOI.

Ali, J., Bakhsh, E.M., Hussain, N., Bilal, M., Akhtar, K., Fagieh, T.M., Danish, E.Y., Asiri, A.M., Su, X. and Khan, S.B., 2022. A new biosource for the synthesis of activated carbon and its potential use for removal of methylene blue and eriochrome black T from aqueous solutions. *Industrial Crops and Products*, 179, p.114676. DOI.

Al-Ma'abreh, A.M., AlKhabbas, M., Alawaideh, S., Hussein-Al-Ali, S.H., Hmedat, D.A., Edris, G., Abuassaf, R.A. and Hamed, M.A., 2024. Investigation of kinetics, thermodynamics, and isotherms of the simultaneous removal of heavy metal ions by activated carbon from cypress fruit. *Adsorption Science & Technology*, 42, pp.1-15. DOI.

Alonso-Magdalena, P., Tudurí, E., Marroquí, L., Quesada, I., Sargis, R.M. and Nadal, A., 2019. Toxic Effects of Common Environmental Pollutants in Pancreatic β-Cells and the Onset of Diabetes Mellitus. *Encyclopedia of Endocrine Diseases*, pp.764–775. DOI.

Ayuba, A.M. and Sani, M., 2022. Removal of Eriochrome Black T dye from aqueous solution using base-activated typha grass (*Typha latifolia*) as an adsorbent. *Bayero Journal of Pure and Applied Sciences*, 15 (1), pp.95–104. DOI.

Azari, A., Noorisepehr, M., Dehganifard, E., Karimyan, K., Hashemi, S.Y., Kalhori, E.M., Norouzi, R., Agarwal, S. and Gupta, V.K., 2019. Experimental design, modeling, and mechanism of cationic dyes biosorption onto magnetic chitosan-glutaraldehyde composite. *International Journal of Biological Macromolecules*, 131, pp.633–645. DOI.

Aziz, M.A., Chowdhury, I.R., Mazumder, M.A.J. and Chowdhury, S., 2019. Highly porous carboxylated activated carbon from jute stick for removal of Pb2+ from aqueous solution. *Environmental Science and Pollution Research*, 26 (22), pp.22656–22669. DOI.

Bello, K., Sarojini, B.K., Narayana, B., Rao, A. and Byrappa, K., 2018. A study on adsorption behavior of newly synthesized banana pseudo-stem derived superabsorbent hydrogels for cationic and anionic dye removal from effluents. *Carbohydrate Polymers*, 181, pp.605–615. DOI.

Beyan, S.M., Ambio, T.A., Sundramurthy, V.P., Gomadurai, C. and Getahun, A.A., 2024. Adsorption Phenomenon for Removal of Pb (II) via Teff Straw-based Activated Carbon Prepared by Microwave-Assisted Pyrolysis: Process Modelling, Statistical Optimisation, Isotherm, Kinetics, and Thermodynamic Studies. *International Journal of Environmental Analytical Chemistry*, 104 (4), pp.916–937. DOI.

Bumajdad, A. and Hasila, P., 2023. Surface modification of date palm-activated carbonaceous materials for heavy metal removal and CO2 adsorption. *Arabian Journal of Chemistry*, 16 (1), p.104403. DOI.

Chen, Q., Yao, Y., Li, X., Lu, J., Zhou, J. and Huang, Z., 2018. Comparison of heavy metal removals from aqueous solutions by chemical precipitation and characteristics of precipitates. *Journal of Water Process Engineering*, 26, pp.289–300. DOI.

Cunha, M.R., Lima, E.C., Lima, D.R., da Silva, R.S., Thue, P.S., Seliem, M.K., Sher, F., dos Reis, G.S. and Larsson, S.H., 2020. Removal of captopril pharmaceutical from synthetic pharmaceutical-industry wastewaters: Use of activated carbon derived from *Butia catarinensis*. *Journal of Environmental Chemical Engineering*, 8 (6), p.104506. DOI.

Danish, M., Ahmad, T., Hashim, R., Said, N., Akhtar, M.N., Mohamad-Saleh, J. and Sulaiman, O., 2018. Comparison of surface properties of wood biomass activated carbons and their application against rhodamine B and methylene blue dye. *Surfaces and Interfaces*, 11, pp.1–13. DOI.

Dobrowolski, R., Krzyszczak, A., Dobrzyńska, J., Podkościelna, B., Zięba, E., Czemierska, M., Jarosz-Wilkołazka, A. and Stefaniak, E.A., 2019. Extracellular polymeric substances are immobilized on microspheres for the removal of heavy metals from an aqueous environment. *Biochemical Engineering Journal*, 143, pp.202–211. DOI.

Doggaz, A., Attoura, A., le Page Mostefa, M., Côme, K., Tlili, M. and Lapicque, F., 2019. Removal of heavy metals by electrocoagulation from hydrogen carbonate-containing waters: Compared cases of divalent iron and zinc cations. *Journal of Water Process Engineering*, 29, p.100796. DOI.

DOLAŞ, H., 2023. The Adsorption of Eriochrome Black T onto the Activated Carbon Produced from Pepper Stalks. *Journal of Engineering Technology and Applied Sciences*, 8 (2), pp.107–118. DOI.

Donohue, M.D. and Aranovich, G.L., 1998. Adsorption Hysteresis in Porous Solids. *Journal of Colloid and Interface Science*, 205 (1), pp.121–130. DOI.

dos Santos, C.C., Mouta, R., Junior, M.C.C., Santana, S.A.A., Silva, H.A. dos S. and Bezerra, C.W.B., 2018. Chitosan-edible oil-based materials as upgraded adsorbents for textile dyes. *Carbohydrate Polymers*, 180, pp.182–191. DOI.

Du, W.N. and Chen, S.T., 2018. Photo- and chemocatalytic oxidation of dyes in water. *Journal of Environmental Management*, 206, pp.507–515. DOI.

El Mansouri, F., Pelaz, G., Morán, A., Da Silva, J.C.G.E., Cacciola, F., El Farissi, H., Tayeq, H., Zerrouk, M.H. and Brigui, J., 2022. Efficient Removal of Eriochrome Black T Dye Using Activated Carbon of Waste Hemp (*Cannabis sativa* L.) Grown in Northern Morocco Enhanced by New Mathematical Models. *Separations*, 9 (10), p.283. DOI.

Eletta, O.A.A., Ayandele, F.O. and Ighalo, J.O., 2023. Adsorption of Pb (II) and Fe (II) by mesoporous composite activated carbon from *Tithonia diversifolia* stalk and *Theobroma cacao* pod. *Biomass Conversion and Biorefinery*, 13 (11), pp.9831–9840. DOI.

Elizalde-González, M.P. and Hernández-Montoya, V., 2009. Use of Wide-Pore Carbons to Examine IntermoLecular Interactions during the Adsorption of Anthraquinone Dyes from Aqueous Solution: *Adsorption Science & Technology*, 27 (5), pp.447–459. DOI.

Faria, P.C.C., Órfão, J.J.M. and Pereira, M.F.R., 2004. Adsorption of anionic and cationic dyes on activated carbons with different surface chemistries. *Water Research*, 38 (8), pp.2043–2052. DOI.

Feng, Y., Yang, S., Xia, L., Wang, Z., Suo, N., Chen, H., Long, Y., Zhou, B. and Yu, Y., 2019. In-situ ion exchange electrocatalysis biological coupling (i-IEEBC) for simultaneously enhanced degradation of organic pollutants and heavy metals in electroplating wastewater. *Journal of Hazardous Materials*, 364, pp.562–570. DOI.

Ghobashy, M.M. and Elhady, M.,. A., 2017. pH-sensitive wax emulsion

copolymerization with acrylamide hydrogel using gamma irradiation for dye removal. *Radiation Physics and Chemistry*, 134, pp.47–55. DOI.

Gupta, N.K., Gupta, A., Ramteke, P., Sahoo, H. and Sengupta, A., 2019. Biosorption-a green method for the preconcentration of rare earth elements (REEs) from waste solutions: A review. *Journal of Molecular Liquids*, 274, pp.148–164. DOI.

Gupta, N.K., Sengupta, A., Gupta, A., Sonawane, J.R. and Sahoo, H., 2018. Biosorption-an alternative method for nuclear waste management: A critical review. *Journal of Environmental Chemical Engineering*, 6 (2), pp.2159–2175. DOI.

Hosseini, S.A., Vossoughi, M., Mahmoodi, N.M. and Sadrzadeh, M., 2018. Efficient dye removal from aqueous solution by high-performance electrospun nanofibrous membranes through the incorporation of SiO_2 nanoparticles. *Journal of Cleaner Production*, 183, pp.1197–1206. DOI.

Hou, T., Du, H., Yang, Z., Tian, Z., Shen, S., Shi, Y., Yang, W. and Zhang, L., 2019. Flocculation of different types of combined contaminants of antibiotics and heavy metals by thermo-responsive flocculants with various architectures. *Separation and Purification Technology*, 223, pp.123–132. DOI.

Hufton, J., Harding, J., Smith, T. and Romero-González, M.E., 2021. The importance of the bacterial cell wall in uranium (VI) biosorption. *Physical Chemistry Chemical Physics*, 23 (2), pp.1566–1576. DOI.

Isam, M., Baloo, L., Chabuk, A., Majdi, A. and Al-Ansari, N., 2024. Optimization and modeling of Pb (II) and Cu (II) adsorption onto red algae (Gracilaria changii)-based activated carbon by using response surface methodology. *Biomass Conversion and Biorefinery*, 14 (15), pp.16799–16818. DOI.

Jacob, J.M., Karthik, C., Saratale, R.G., Kumar, S.S., Prabakar, D., Kadirvelu, K. and Pugazhendhi, A., 2018. Biological approaches to tackle heavy metal pollution: A survey of literature. *Journal of Environmental Management*, 217, pp.56–70. DOI.

Kasperiski, F.M., Lima, E.C., Umpierres, C.S., dos Reis, G.S., Thue, P.S., Lima, D.R., Dias, S.L.P., Saucier, C. and da Costa, J.B., 2018. Production of porous activated carbons from *Caesalpinia ferrea* seed pod wastes: Highly efficient removal of captopril from aqueous solutions. *Journal of Cleaner Production*, 197, pp.919–929. DOI.

Kavitha, E., Sowmya, A., Prabhakar, S., Jain, P., Surya, R. and Rajesh, M.P., 2019. Removal and recovery of heavy metals through size-enhanced ultrafiltration using chitosan derivatives and optimization with response surface modeling. *International Journal of Biological Macromolecules*, 132, pp.278–288. DOI.

Khnifira, M., Boumya, W., Abdennouri, M., Sadiq, M., Achak, M., Serdaroğlu, G., Kaya, S., Şimşek, S. and Barka, N., 2021. A combined molecular dynamic simulation, DFT calculations, and experimental study of the eriochrome black T dye adsorption onto chitosan in aqueous solutions. *International Journal of Biological Macromolecules*, 166, pp.707–721. DOI.

Krstić, V., Urošević, T. and Pešovski, B., 2018. A review on adsorbents for treatment of water and wastewaters containing copper ions. *Chemical Engineering Science*, 192, pp.273–287. DOI.

Li, R., Cao, X., Fan, X., Shi, J., Meng, B., Zhang, J., Wang, Y., Du, J., Deng, X. and Zheng, C., 2024. Study of the Factors Influencing the Adsorption of Heavy Metal Pollutants in Water by Activated Carbon Gel Particles. *Journal of Environmental Engineering*, 150 (7). DOI.

Lima, D.R., Hosseini-Bandegharaei, A., Thue, P.S., Lima, E.C., de Albuquerque, Y.R.T., dos Reis, G.S., Umpierres, C.S., Dias, S.L.P. and Tran, H.N., 2019. Efficient acetaminophen removal from water and hospital effluents treatment by activated carbons derived from Brazil nutshells. *Colloids and Surfaces A: Physicochemical and Engineering Aspects*, 583, p.123966. DOI.

Liu, J., Hu, C. and Huang, Q., 2019. Adsorption of Cu2+, Pb2+, and Cd2+ onto oiltea shell from water. *Bioresource Technology*, 271, pp.487–491. DOI.

Madeła, M. and Skuza, M., 2021. Towards a circular economy: Analysis of the use of biowaste as biosorbent for the removal of heavy metals. *Energies*, 14 (17), pp.5427–5442. DOI.

Mandal, S., Calderon, J., Marpu, S.B., Omary, M.A. and Shi, S.Q., 2021. Mesoporous activated carbon as a green adsorbent for the removal of heavy metals and Congo red: Characterization, adsorption kinetics, and isotherm studies. *Journal of Contaminant Hydrology*, 243, p.103869. DOI.

Melliti, A., Yılmaz, M., Sillanpää, M., Hamrouni, B. and Vurm, R., 2023. Low-cost date palm fiber activated carbon for effective and fast heavy metal adsorption from water: Characterization, equilibrium, and kinetics studies. *Colloids and Surfaces A: Physicochemical and Engineering Aspects*, 672, p.131775. DOI.

Mkilima, T., Zharkenov, Y., Abduova, A., Sarypbekova, N., Kudaibergenov, N., Sakanov, K., Zhukenova, G., Omarov, Z., Sultanbekova, P. and Kenzhaliyeva, G., 2024. Utilization of banana peel-derived activated carbon for the removal of heavy metals from industrial wastewater. *Case Studies in Chemical and Environmental Engineering*, 10, p.100791. DOI.

Mohammed, N.A.S., Abu-Zurayk, R.A., Hamadneh, I. and Al-Dujaili, A.H., 2018. Phenol adsorption on biochar prepared from the pine fruit shells: Equilibrium, kinetic and thermodynamics studies. *Journal of Environmental Management*, 226, pp.377–385. DOI.

Mostafa, N., Eldahshan, O. and Singab, A.N., 2014. The Genus *Jacaranda* (Bignoniaceae): An updated review. *Pharmacognosy Communication*, 4 (3), pp.31–39. DOI.

Moyo, M., Pakade, V.E. and Modise, S.J., 2017. Biosorption of lead (II) by chemically modified *Mangifera indica* seed shells: Adsorbent preparation, characterization and performance assessment. *Process Safety and Environmental Protection*, 111, pp.40–51. DOI.

Napoli, M., Cecchi, S., Grassi, C., Baldi, A., Zanchi, C.A. and Orlandini, S., 2019. Phytoextraction of copper from contaminated soil using arable and vegetable crops. *Chemosphere*, 219, pp.122–129. DOI.

Nemati, M., Hosseini, S.M. and Shabanian, M., 2017. Novel electrodialysis cation exchange membrane prepared by 2-acrylamido-2-methylpropane sulfonic acid; heavy metal ions removal. *Journal of Hazardous Materials*, 337, pp.90–104. DOI.

Özdemir, S., Mohamedsaid, S.A., Kılınç, E. and Soylak, M., 2019. Magnetic solid phase extractions of Co (II) and Hg (II) by using magnetized *C. micaceus* from water and food samples. *Food Chemistry*, 271, pp.232–238. DOI.

Patiño-Rodríguez, O., Agama-Acevedo, E., Ramos-Lopez, G. and Bello-Pérez, L.A., 2020. Unripe mango kernel starch: Partial characterization. *Food Hydrocolloids*, 101, p.105512. DOI.

Qiu, M. and He, C., 2019. Efficient removal of heavy metal ions by forward osmosis membrane with a polydopamine-modified zeolitic imidazolate framework incorporated selective layer. *Journal of Hazardous Materials*, 367, pp.339–347. DOI.

Que, W., Zhou, Y. hui, Liu, Y. guo, Wen, J., Tan, X. fei, Liu, S. and Jiang, L.H., 2019. Appraising the effect of in-situ remediation of heavy metal contaminated sediment by biochar and activated carbon on Cu immobilization and microbial community. *Ecological Engineering*, 127, pp.519–526. DOI.

Ragsac, A.C., Farias-Singer, R., Freitas, L.B., Lohmann, L.G. and Olmstead, R.G., 2019. Phylogeny of the Neotropical tribe Jacarandeae (*Bignoniaceae*). *American Journal of Botany*, 106 (12), pp.1589–1601. DOI.

Rai, D. and Sinha, S., 2022. Research trends in the development of anodes for electrochemical oxidation of wastewater. *Reviews in Chemical Engineering*, 39 (5), pp.807–855. DOI.

Rambabu, K., Bharath, G., Banat, F. and Show, P.L., 2020. Biosorption performance of date palm empty fruit bunch wastes for toxic hexavalent chromium removal. *Environmental Research*, 187, p.109694. DOI.

Rath, J., Sahoo, J.K., Sukla, R.K., Pradhan, A., Biswal, S.K., Dwivedy, P. and Sahoo, S.K., 2024. Eriochrome Black T dye removal from an

aqueous solution using graphene oxide-modified activated carbon materials. *Indian Chemical Engineer*, pp.1–20. DOI.

Reck, I.M., Paixão, R.M., Bergamasco, R., Vieira, M.F. and Vieira, A.M.S., 2018. Removal of tartrazine from aqueous solutions using adsorbents based on activated carbon and *Moringa oleifera* seeds. *Journal of Cleaner Production*, 171, pp.85–97. DOI.

Ren, B., Jin, Y., Zhao, L., Cui, C. and Song, X., 2022. Enhanced Cr (VI) adsorption using chemically modified dormant *Aspergillus niger* spores: Process and mechanisms. *Journal of Environmental Chemical Engineering*, 10 (1), p.106955. DOI.

Sadeghi, S., Zakeri, H.R., Saghi, M.H., Ghadiri, S.K., Talebi, S.S., Shams, M. and Dotto, G.L., 2021. Modified wheat straw–derived graphene for the removal of Eriochrome Black T: characterization, isotherm, and kinetic studies. *Environmental Science and Pollution Research*, 28 (3), pp.3556–3565. DOI.

Salomón, Y.L.D.O., Georgin, J., Franco, D.S.P., Netto, M.S., Piccilli, D.G.A., Foletto, E.L., Oliveira, L.F.S. and Dotto, G.L., 2021. High-performance removal of 2,4-dichlorophenoxyacetic acid herbicide in water using activated carbon derived from Queen palm fruit endocarp (Syagrus romanzoffiana). *Journal of Environmental Chemical Engineering*, 9 (1), p.104911. DOI.

Sandhu, K.S. and Lim, S.T., 2008. Structural characteristics and in vitro digestibility of Mango kernel starch (Mangifera indica L.). *Food Chemistry*, 107 (1), pp.92–97. DOI.

Sing, K.S.W., Everett, D.H., Haul, R.A.W., Moscou, L., Pierotti, R.A., Rouquerol, J. and Siemieniewska, T., 1985. Reporting physisorption data for gas/solid systems with special reference to the determination of surface area and porosity. *Pure and Applied Chemistry*, 57 (4), pp.603–619. DOI.

Thommes, M., Kaneko, K., Neimark, A. v., Olivier, J.P., Rodriguez-Reinoso, F., Rouquerol, J. and Sing, K.S.W., 2015. Physisorption of gases, with special reference to the evaluation of surface area and pore size distribution (IUPAC Technical Report). *Pure and Applied Chemistry*, 87 (9–10), pp.1051–1069. DOI.

Tonato, D., Drumm, F.C., Grassi, P., Georgin, J., Gerhardt, A.E., Dotto, G.L. and Mazutti, M.A., 2019. Residual biomass of *Nigrospora* sp. from the process of microbial oil extraction for the biosorption of procion red H–E7B dye. *Journal of Water Process Engineering*, 31, p.100818. DOI.

Treviño-Cordero, H., Juárez-Aguilar, L.G., Mendoza-Castillo, D.I., Hernández-Montoya, V., Bonilla-Petriciolet, A. and Montes-Morán, M.A., 2013. Synthesis and adsorption properties of activated carbons from biomass of *Prunus domestica* and *Jacaranda mimosifolia* for the removal of heavy metals and dyes from water. *Industrial Crops and Products*, 42 (1), pp.315–323. DOI.

Wei, Y., Salih, K.A.M., Rabie, K., Elwakeel, K.Z., Zayed, Y.E., Hamza, M.F. and Guibal, E., 2021. Development of phosphoryl-functionalized algal-PEI beads for the sorption of Nd (III) and Mo (VI) from aqueous solutions – Application for rare earth recovery from acid leachates. *Chemical Engineering Journal*, 412, p.127399. DOI.

Yao, T., Qiao, L. and Du, K., 2020. High tough and highly porous graphene/carbon nanotubes hybrid beads enhanced by carbonized polyacrylonitrile for efficient dye adsorption. *Microporous and Mesoporous Materials*, 292, p.109716. DOI.

Yin, K., Wang, Q., Lv, M. and Chen, L., 2019. Microorganism remediation strategies towards heavy metals. *Chemical Engineering Journal*, 360, pp.1553–1563. DOI.